

## Thermally activated precipitation at deformation-induced defects in Fe-Cu and Fe-Cu-B-N alloys studied by positron annihilation spectroscopy

S. M. He,<sup>1,\*</sup> N. H. van Dijk,<sup>1</sup> H. Schut,<sup>2</sup> E. R. Peekstok,<sup>3</sup> and S. van der Zwaag<sup>4</sup>

<sup>1</sup>*Fundamental Aspects of Materials and Energy, Faculty of Applied Sciences, Delft University of Technology, Mekelweg 15, 2629 JB Delft, The Netherlands*

<sup>2</sup>*Neutron and Positron Methods in Materials, Faculty of Applied Sciences, Delft University of Technology, Mekelweg 15, 2629 JB Delft, The Netherlands*

<sup>3</sup>*Microstructural Control in Metals (MCM), Mechanical, Maritime and Materials Engineering, Delft University of Technology, Mekelweg 2, 2628 CD Delft, The Netherlands*

<sup>4</sup>*Novel Aerospace Materials Group, Faculty of Aerospace Engineering, Delft University of Technology, Kluijverweg 1, 2629 HS Delft, The Netherlands*

(Received 17 September 2009; revised manuscript received 8 February 2010; published 10 March 2010)

We have investigated the influence of deformation-induced defects on the isothermal precipitation at 550 °C in as-quenched (solute-supersaturated) and annealed (solute-depleted) Fe-Cu and Fe-Cu-B-N alloys by positron annihilation spectroscopy and hardness tests. Using the coincidence Doppler broadening technique, the evolution of local environment at the positron annihilation sites (open-volume defects, Cu precipitates, and matrix) was monitored as a function of the aging time. For all samples, plastic deformation causes a pronounced change in  $S$  and  $W$  parameters signaling the formation of open-volume defects. For the as-quenched samples, aging results in a sharp decrease in the amount of open-volume defects combined with the rise of a strong copper signature, which can be attributed to preferential copper precipitation at the open-volume defects introduced by plastic deformation. In contrast, the open-volume defects of the annealed samples can only be reduced partially. Both the hardness tests and the positron annihilation spectroscopy indicate that the addition of B and N to the Fe-Cu alloy causes a significant acceleration of the precipitation in the as-quenched alloys.

DOI: [10.1103/PhysRevB.81.094103](https://doi.org/10.1103/PhysRevB.81.094103)

PACS number(s): 61.66.Dk, 61.72.-y, 64.75.-g, 65.80.-g

### I. INTRODUCTION

Steels are among the most widely used construction materials as their mechanical properties can be tailored to obtain the required combination of strength and formability. However, in highly demanding applications, the lifetime of steels is limited due to the accumulation of damage. This damage causes the formation of ultrafine cracks that subsequently grow and finally lead to fracture of the components.

Recently it was realized that creep damage can be self-healed in boron- and copper-containing austenitic stainless steels by dynamic precipitation of these elements from the supersaturated matrix, resulting in a significant improvement in the creep lifetime.<sup>1-3</sup> The precipitates partially fill the nanoscale open-volume defects and thereby prevent further growth. Self-healing is a promising new approach in the design of future steels with a longer component lifetime.

In order to fully understand the role of these alloying elements and the influence of thermomechanical history on the defect-induced precipitation responsible for self-healing, additional studies on less complex low-alloyed steel grades are desirable. Therefore, high-purity Fe-Cu and Fe-Cu-B-N model alloys have been prepared in order to identify the physical mechanism responsible for self-healing in ferritic steels (body-centered-cubic matrix) and subsequently apply the results to introduce these concepts in industrially steel grades.

The precipitation of copper from supersaturated Fe-Cu alloys has been investigated extensively, both experimentally<sup>4-17</sup> and theoretically.<sup>18-21</sup> It is now generally accepted that, in the initial stages, fully coherent Cu precipitates

inherit the body-centered-cubic (bcc) structure of the  $\alpha$ -Fe matrix. When reaching a critical diameter of approximately 4–6 nm, the growing bcc precipitates undergo a martensitic transformation to a less coherent  $9R$  structure. At sizes larger than 15–17 nm, a second transformation to the more stable  $3R$  structure takes place before the Cu precipitates adopt their final equilibrium face-centered cubic (fcc) structure. The full transformation sequence for copper precipitation in Fe-Cu alloys is given by  $\text{bcc} \rightarrow 9R \rightarrow 3R \rightarrow \text{fcc}$  for increasing aging time. As far as the composition of Cu precipitates is concerned, the Cu precipitates are almost pure Cu at sizes above 4–5 nm, but there exists contradicting information about the initial stage of the precipitation process. Investigations performed with atom probe analysis consistently report that the early Cu precipitates contain a significant fraction of Fe (in some cases, even in excess of 50 at. %),<sup>8-11</sup> which was later supported by thermodynamic calculations.<sup>21</sup> This technique, nevertheless, can generate a large statistical error and underestimate the solute concentration in small precipitates due to the finite probe resolution. In contrast, results obtained with small-angle neutron scattering (SANS) (Refs. 12–14) and positron annihilation<sup>15-17</sup> suggest that the precipitates are almost pure Cu with only minor amounts of Fe. Interpretation of the SANS experiments however depends on *a priori* knowledge of the magnetic state and the atom density of the small Cu clusters, which causes some uncertainty in the determination of the composition of the Cu precipitates in the initial stage of the precipitation process. The composition of the metastably ultrafine bcc precipitate in the Fe-Cu system is therefore still an open question.

TABLE I. Chemical composition of the studied high-purity model alloys (in wt %) with balance iron. The Ce content refers to the added nominal composition.

Alloy	Cu	B	N	C	S	Ce
Fe-Cu	1.11	<0.01	0.002	0.0056	0.002	0.015
Fe-Cu-B-N	1.06	0.052	0.029	0.0032	0.002	0.015

So far, however, limited information is available on the influence of open-volume defects and/or additional alloying elements on the Cu precipitation. It is well known that open-volume defects (vacancies, vacancy clusters, and dislocations) facilitate the diffusion of solutes and thereby accelerate the precipitation, which is expected to promote the self-healing of metals by dynamic precipitation. Dislocations, which are easily multiplied by deformation, are found to accelerate the diffusion of impurities by almost 3 orders of magnitude compared to bulk diffusion.<sup>22</sup>

Positron annihilation is one of the few techniques that can probe the evolution of open-volume defects and nanoscale precipitates within the bulk of the material. Nagai and co-workers<sup>23</sup> monitored the copper precipitation of an undeformed Fe-Cu (1.0 wt %) alloy by the evolution of the coincidence Doppler broadening (CDB) spectra during thermal aging at 550 °C for aging times from 0.1 to 312 h. Subsequently, Onitsuka and co-workers<sup>24</sup> studied the effect of rolling deformation on the isochronal precipitation of the Fe-Cu (1.0 wt %) alloy by positron annihilation spectroscopy. They observed the formation of Cu-vacancy clusters and proposed that the diffusion of Cu atoms was enhanced by deformation-induced excess vacancies that are mobile at room temperature. In addition, the interaction of irradiation-induced vacancies and Cu aggregations in Fe-Cu model alloys was studied by Nagai and co-workers<sup>25</sup> and by Hasegawa and co-workers.<sup>26</sup> They concluded that the irradiation results in a vacancy-solute complex that speeds up the precipitation. These irradiation studies however give limited insight in the deformation-induced precipitation as the main defects in iron induced by deformation are dislocations rather than vacancies.<sup>27,28</sup>

Although the binary Fe-Cu alloys have been widely studied, little is known about the effect of microalloying of copper-containing alloys with boron and nitrogen. The addition of boron and nitrogen was found to suppress creep cavity growth in copper-containing stainless steels leading to a higher rupture strength and a higher rupture ductility.<sup>3</sup> The effect of boron and nitrogen on the copper precipitation mechanism was however not clarified.

In order to establish the potential for self-healing of defect-induced precipitation and the role of added boron and nitrogen in copper-based iron alloys, we have investigated the isothermal Cu precipitation at 550 °C in high-purity Fe-Cu and Fe-Cu-B-N alloys after tensile deformation by positron annihilation spectroscopy measurements and hardness tests. Employing as-quenched (solute-supersaturated) and annealed (solute-depleted) samples, a quantitative analysis of contributions from the three positron annihilation sites, i.e., open-volume defects, Cu precipitates, and matrix, has been performed by fitting the CDB spectra measured before

deformation, after deformation, and for aging times up to 96 h by a linear combination of the reference spectra.

## II. EXPERIMENTAL

In our studies, we compared the precipitation kinetics in deformed Fe-Cu and Fe-Cu-B-N alloys by positron annihilation spectroscopy. The chemical composition of the investigated alloys is listed in Table I. For comparison, pure Fe (99.99+ %purity) was used. All alloys were produced in sheets of 10×10 cm<sup>2</sup> with a thickness of 0.5 mm by Goodfellow. From this material, dog-bone (I)-shaped samples were cut by spark erosion for tensile deformation tests. The samples were solution-treated at 850 °C for 1 h in evacuated silica tubes filled with 200 mbar ultrahigh purity (uhp) argon gas and subsequently quenched into water. For the as-quenched (AQ) samples, the alloys are in a supersaturated state. Before aging at 550 °C, part of the samples was subsequently annealed at 700 °C for 2 h and cooled at a very slow rate of 20 °C/h in a vacuum furnace ( $<3 \times 10^{-4}$  Pa). For the annealed (Ann) samples, most of the solutes are believed to be depleted in the alloys. Part of the samples was subjected to tensile deformation up to a strain of 8% in a 2 kN microtensile tester (Deben).

Hardness tests were performed on samples that were aged for 0–100 h at a temperature of 550 °C in a salt bath. For the hardness tests, a Buehler microhardness tester was used with a Vickers microhardness indenter, a load of 4.9 N, and a holding time of 15 s. Before the optical microstructure observations, the specimens were etched in a 2 vol % nital solution. In order to perform positron measurements for varying aging times, the samples were heated in a vacuum furnace ( $<3 \times 10^{-4}$  Pa) to a temperature of 550 °C for increasing aging times between the positron experiments.

The coincidence Doppler broadening spectra were measured by using a <sup>22</sup>Na positron source and two HPGe detectors to record both annihilation photons in coincidence. Compared to single detector Doppler broadening measurement, this gives a much better peak-to-background ratio ( $\sim 10^5$ ) with an energy resolution of 1 keV at 511 keV. This resolution corresponds to a momentum resolution of  $4 \times 10^{-3} m_0 c$  (full width at half maximum, FWHM), where  $c$  is the velocity of light and  $m_0$  is the electron rest mass. The activity of the used <sup>22</sup>Na positron source was about 2 MBq. Total counts of more than  $1.5 \times 10^6$  were accumulated for each spectrum.

By measuring the Doppler shift in the energy of the 511 keV annihilation gamma quanta, information about the momentum distribution of the electrons, involved in the positron annihilation, is obtained. All the measured coincidence Doppler broadening spectra were divided by the spectrum of the

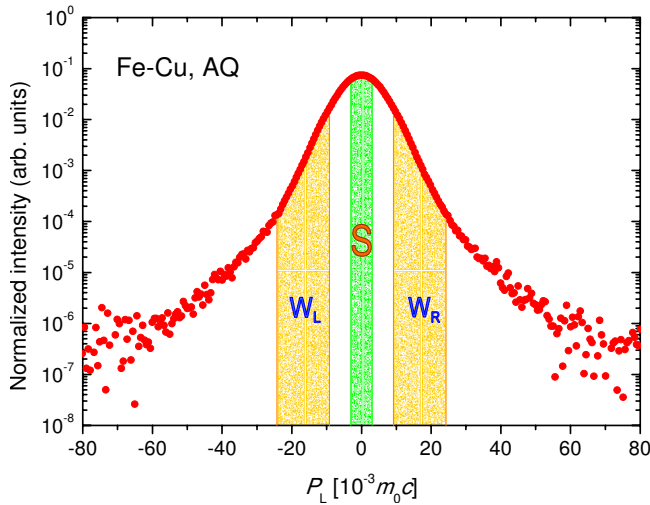


FIG. 1. (Color online) Coincidence Doppler broadening spectrum of the undeformed as-quenched Fe-Cu alloy as a function of the electron momentum  $p_L$ . The line-shape parameters  $S$  and  $W$  are determined by the indicated areas  $A_S$  and  $A_W$  divided by the area below the whole curve.

reference material, i.e., defect-free pure Fe. The shape of the curve in the high-momentum region ( $|p_L| > 10 \times 10^{-3} m_0 c$ ) of the thus-obtained relative momentum distributions exhibits the characteristic features of positrons annihilating with their inner orbital electrons and thus gives insight in the elemental configuration at the annihilation site. In its simplest form, two parameters ( $S$  and  $W$ ) are derived from the Doppler-broadened 511-keV photon peak reflecting a one-dimensional projection of the three-dimensional momentum distributions of the annihilating positron-electron pairs.<sup>25,29</sup>

The  $S$  (shape) parameter represents annihilations with (low-momentum) valence electrons and is calculated as the ratio of the number of counts in a fixed momentum window ( $|p_L| < 3.1 \times 10^{-3} m_0 c$ ) around the center of the peak to the total counts. Similarly, the  $W$  (wing) parameter is obtained from the contribution of annihilations with high-momentum core electrons in the interval  $9.2 \times 10^{-3} m_0 c < |p_L| < 24.3 \times 10^{-3} m_0 c$ . Figure 1 shows an example of a measured momentum spectrum with the regions from which the  $S$  and  $W$  parameters are calculated. At open-volume defects, the probability of annihilations with high-momentum core electrons is locally decreased. This results in a higher  $S$  parameter and a lower  $W$  parameter.

### III. RESULTS AND DISCUSSIONS

#### A. Aging curves

In Fig. 2, the effect of aging at a temperature of 550 °C on the hardness for the as-quenched Fe-Cu and Fe-Cu-B-N alloys with and without an 8% plastic predeformation is shown. For the undeformed alloys, the typical age-hardening behavior for copper precipitation is observed. The peak hardness is reached at about 6 h for the Fe-Cu alloy and 4 h for the Fe-Cu-B-N alloy. The 8% plastic predeformation leads to a significant increase in the initial hardness caused by cold-

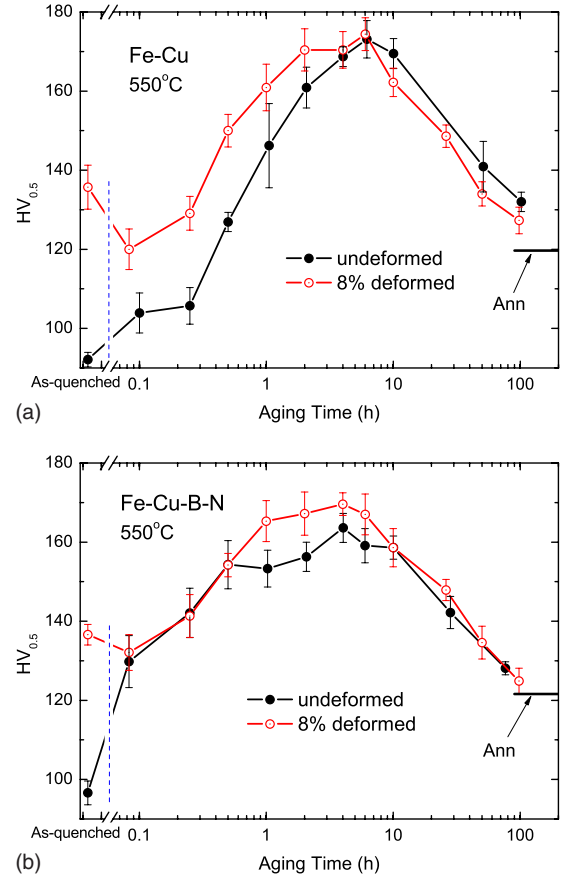


FIG. 2. (Color online) Hardness aging curves of the as-quenched samples aged at 550 °C with and without 8% predeformation.

work hardening, which reduces during aging. For the Fe-Cu alloy, the hardness of the deformed sample with 8% prestrain slightly decreases in the initial stage of aging due to the recovery of dislocations. The hardness subsequently increases rapidly and stays above that of the undeformed sample in the underaged and peak-aged regime, but seems to be below it in the overaged stage. For the Fe-Cu-B-N alloy, the hardness of the deformed sample is higher than that of undeformed sample in the peak-aged regime, while the aging curves almost overlap in the underaged and overaged regimes.

A comparison of the aging behavior of both alloys in Fig. 2 indicates that the Fe-Cu-B-N alloy has a faster response than the Fe-Cu alloy. This means that the precipitation of Fe-Cu alloy is accelerated by the addition of B and N. The time to reach peak hardness was found to be relatively insensitive to the predeformation: only for the Fe-Cu alloy the predeformation seems to result in a minor reduction in the time to reach peak hardness. For comparison, the hardness of the (undeformed) annealed samples is indicated by the solid line on the right side of the figures. For both alloys, the annealed samples have a higher hardness than the as-quenched by over 20 Vickers hardness numbers, which is comparable to the extrapolated values expected for aging times of about 200 h.

The results for the Fe-Cu alloy with 1.1 wt % Cu are in good agreement with earlier hardness studies on binary

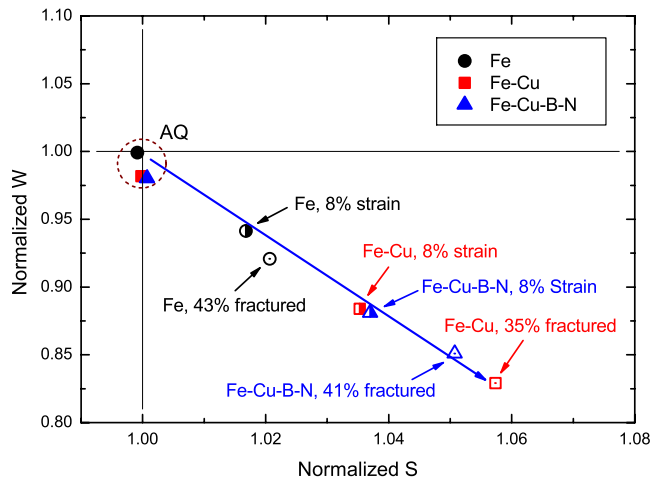


FIG. 3. (Color online) Effect of the strain level on the  $S$  and  $W$  parameters of the as-quenched Fe-Cu and Fe-Cu-B-N alloys and pure Fe. The plastic tensile deformation leads to the formation of open-volume defects.

Fe-Cu alloys.<sup>12,30–32</sup> Both the peak hardness and the aging time to peak are in between those reported for 0.8 wt % Cu (Ref. 30) and for 1.3 wt % Cu,<sup>12</sup> and very close to that reported for 1.0 wt % Cu.<sup>32</sup> The observed effect of prestrain on the hardness during aging is consistent with that observed by Deschamps and co-workers.<sup>30</sup>

## B. Positron annihilation

### 1. Evaluation of the $S$ and $W$ parameters

Figure 3 shows the  $S$  and  $W$  parameters measured for the as-quenched samples, the 8% deformed samples, and the fractured samples. All  $S$ - $W$  couples are normalized to that of annealed pure iron ( $S=0.466$  and  $W=0.118$ ). As indicated in Fig. 3, the  $S$ - $W$  couples of all the as-quenched alloys and the annealed pure iron are very close to that of as-quenched pure iron. This confirms earlier reports<sup>33</sup> that it is difficult to form open-volume defects in iron by thermal processes. The  $S$ - $W$  couples of the deformed samples show a common linear behavior:  $S$  increases and  $W$  decreases with increasing strain levels. This means that in all the investigated alloys, the same types of defects (predominantly dislocations) are generated by tensile deformation. Among the  $S$ - $W$  couples of fractured tensile samples, the Fe-Cu alloy exhibits the largest shift. In Fig. 4, the  $S$ - $W$  couples of pure iron are shown after deformation and subsequent aging at 550 °C for 15 min. After aging, the  $S$ - $W$  couples of the deformed as-quenched and annealed samples almost return to their initial position. This suggests that the open-volume defects introduced by plastic deformation can be recovered almost completely (>93%, calculated from the change in  $S$  parameter) by self-diffusion of Fe atoms during the aging step (independent of the heat treatment before the tensile deformation).

In Fig. 5, the evolution of the normalized  $S$ - $W$  couples (normalized to the value of annealed pure Fe) of the Fe-Cu and Fe-Cu-B-N alloys is shown after tensile deformation and subsequent aging. For the as-quenched samples, both alloys

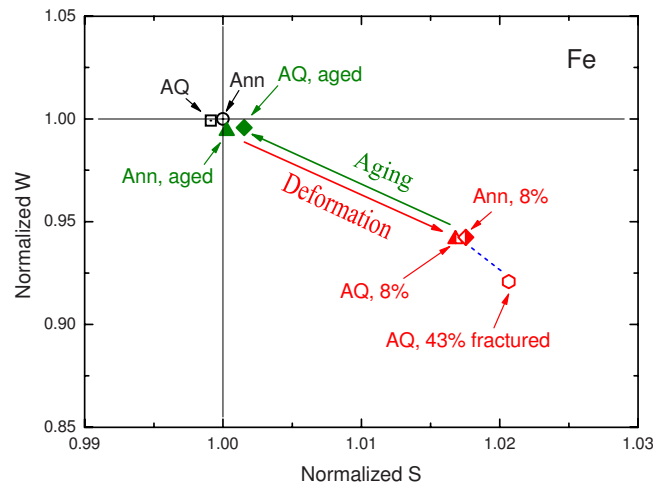


FIG. 4. (Color online) Effect of applied strain (8% and 43%) and subsequent aging for 15 min at 550 °C on the  $S$  and  $W$  parameters of pure Fe for AQ and Ann samples.

show an obvious recovery of the change in  $S$  parameter induced by deformation during the initial stage of the subsequent aging. In addition, the  $W$  parameter strongly increases during aging and approaches the value obtained for pure Cu after an aging time of 1–2 h for the Fe-Cu alloy and 0.25–0.5 h for the Fe-Cu-B-N alloy. For longer aging times, a clear shift in  $S$ - $W$  couples is observed toward the point associated with open-volume defects. For undeformed Fe-Cu with a similar composition, the turn in  $S$ - $W$  couples was observed at a significantly longer aging time of 10 h,<sup>23</sup> indicating the Cu precipitation is promoted by the presence of dislocations introduced by predeformation. The difference in evolution of the  $S$ - $W$  couples during aging for both as-quenched alloys shows that the precipitation kinetics of the Fe-Cu-B-N alloy is faster than that of the Fe-Cu alloy, suggesting that the diffusion of Cu is promoted by the addition of B and N. The mechanism responsible for the accelerated Cu precipitation by added B and N is still ambiguous. A possible explanation for the accelerated Cu precipitation in the Fe-Cu-B-N samples may be that the dislocations created by prestrain are filled with N and/or B. This can prevent decoration of dislocations with copper and thereby leads to a higher effective Cu concentration in the matrix in comparison to the Fe-Cu system. The presence of N and/or B at interfaces and dislocations is also expected to significantly reduce the interfacial energy and can thereby lower the energy barrier for Cu nucleation.

It is interesting to note that positrons are not trapped by the isolated Cu atoms in the supersaturated as-quenched Fe-Cu alloy, but evidently are trapped by the Cu clusters (precipitates). Since the positron affinity of Cu is about 1 eV lower than that of Fe,<sup>34</sup> the Cu cluster can be regarded as a potential well with a depth of 1 eV for the positron. When the size of the potential well is larger than the zero-point motion of the positron, the positron can be trapped in a bound state. For a spherical Cu cluster, the positron can only be trapped when the diameter of the cluster is larger than 0.6 nm.<sup>23,25</sup> In the initial stage of aging, the copper precipitates have the same bcc structure as the Fe-Cu matrix and there-

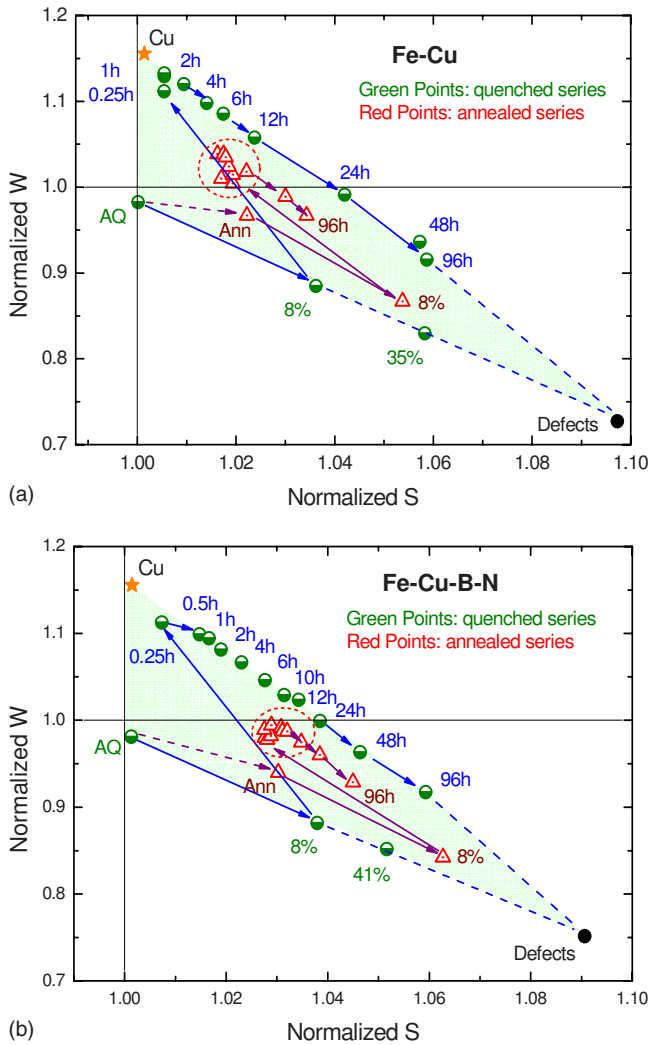


FIG. 5. (Color online) *S*-*W* plots of Fe-Cu and Fe-Cu-B-N alloys as a function of aging time at 550 °C after 8% deformation for AQ and Ann samples.

fore they are completely coherent with matrix.

For the Fe-Cu alloy, the precipitates reach the critical size for the martensitic transformation from bcc structure to the less-coherent 9*R* structure after an aging time of 1 h. This change in structure leads to the formation of open-volume defects at the interface of the precipitate. Thus, the change in behavior for aging times longer than 1 h for the Fe-Cu alloy can be regarded as the onset of bcc → 9*R* phase transformation. The semicoherent precipitates with a 9*R* structure continue to transform upon growth into a transitional 3*R* structure and finally reach the equilibrium fcc structure which has an incoherent interface with the bcc matrix. This sequence of transformations during aging results in an increasing misfit accompanied by the formation of open-volume defects at the interface between the precipitates and matrix. Our positron data suggest a similar precipitation sequence for the Fe-Cu-B-N alloy.

For the annealed samples, the position of aged *S*-*W* couples changes little until an aging time of 12 h is reached. Similar to the as-quenched alloys, for longer aging times, the *S* and *W* values move into the direction of those for the

open-volume defects. The *S*-*W* couples for the open-volume defect reference points of the Fe-Cu and Fe-Cu-B-N alloys are presented at the lower right corners of Figs. 5(a) and 5(b), respectively. As seen from Fig. 5, all the *S*-*W* couples for the Fe-Cu and Fe-Cu-B-N alloys are confined by a triangular region defined by the reference points of annealed Fe, annealed Cu, and open open-volume defects. The reference point of open-volume defects roughly corresponds to the crossing of the lines representing deformation and prolonged aging of the as-quenched alloys. The quantitative determination of these reference points will be discussed in the next section.

2. Decomposition of the coincidence Doppler broadening spectra

A quantitative analysis of the evolution of open defects during Cu precipitation and the coherency loss is of significant importance for the development of the strengthening theory<sup>14,30,35</sup> and clarification of the self-healing mechanism. As discussed in the previous section, the *S*-*W* couples give a qualitative indication of the evolution of Cu precipitates and open-volume defect signatures of the positron trapping sites. However, for a quantitative analysis, a detailed analysis of the whole coincidence Doppler broadening spectra is required.

Figure 6 shows the momentum spectra of the Fe-Cu and Fe-Cu-B-N alloys obtained from the coincidence Doppler broadening measurements. Data are plotted as the relative difference  $(\rho - \rho_{Fe}) / \rho_{Fe}$  of the momentum spectrum  $\rho$  with respect to the momentum spectrum obtained for annealed pure iron  $\rho_{Fe}$  as a function of the electron momentum  $p_L$ . In Figs. 6(a) and 6(b), the ratio curves are shown for the Fe-Cu and the Fe-Cu-B-N alloys, respectively. For clarity, an enlargement of the low-momentum region ( $|p_L| \leq 10^{-2} m_0 c$ ) is shown in Figs. 6(c) and 6(d) for both alloys. In order to estimate the contributions from annihilations at Cu precipitates and of open-volume defects, the ratio curves of the annealed pure Cu and the fully strained (until fracture) alloys are also measured.

The as-quenched alloys exhibit a ratio curve that is virtually zero over the whole momentum range. The subsequent 8% tensile deformation results in a ratio curve that closely resembles a scaled version of the maximum deformed sample, indicating a continuous built up of defects in correspondence with the behavior of the *S*-*W* couples in Fig. 3. For the Fe-Cu alloy, aging of the deformed sample gives rise to a rapid change around  $24 \times 10^{-3} m_0 c$ , indicating the appearance of a copper signature. For aging times up to 1 h, the peak around  $24 \times 10^{-3} m_0 c$ , characteristic for the 3*d* electrons of pure copper,<sup>36</sup> grows with the aging time. The Cu peak was found to reach a maximum at an aging time of about 1 h and then descends with further aging. It is interesting to note that the ratio curve of the deformed Fe-Cu alloy after 1 h of aging almost overlaps that of pure Cu, indicating that nearly all positrons annihilate with Cu electrons. In the low-momentum region [Fig. 6(c)], a continuous rise with aging time is observed after 1 h, indicating a growing contribution from open-volume defects. For the Fe-Cu-B-N alloy, a similar behavior as for the Fe-Cu alloy is observed with faster precipitation kinetics. This behavior is consistent with the

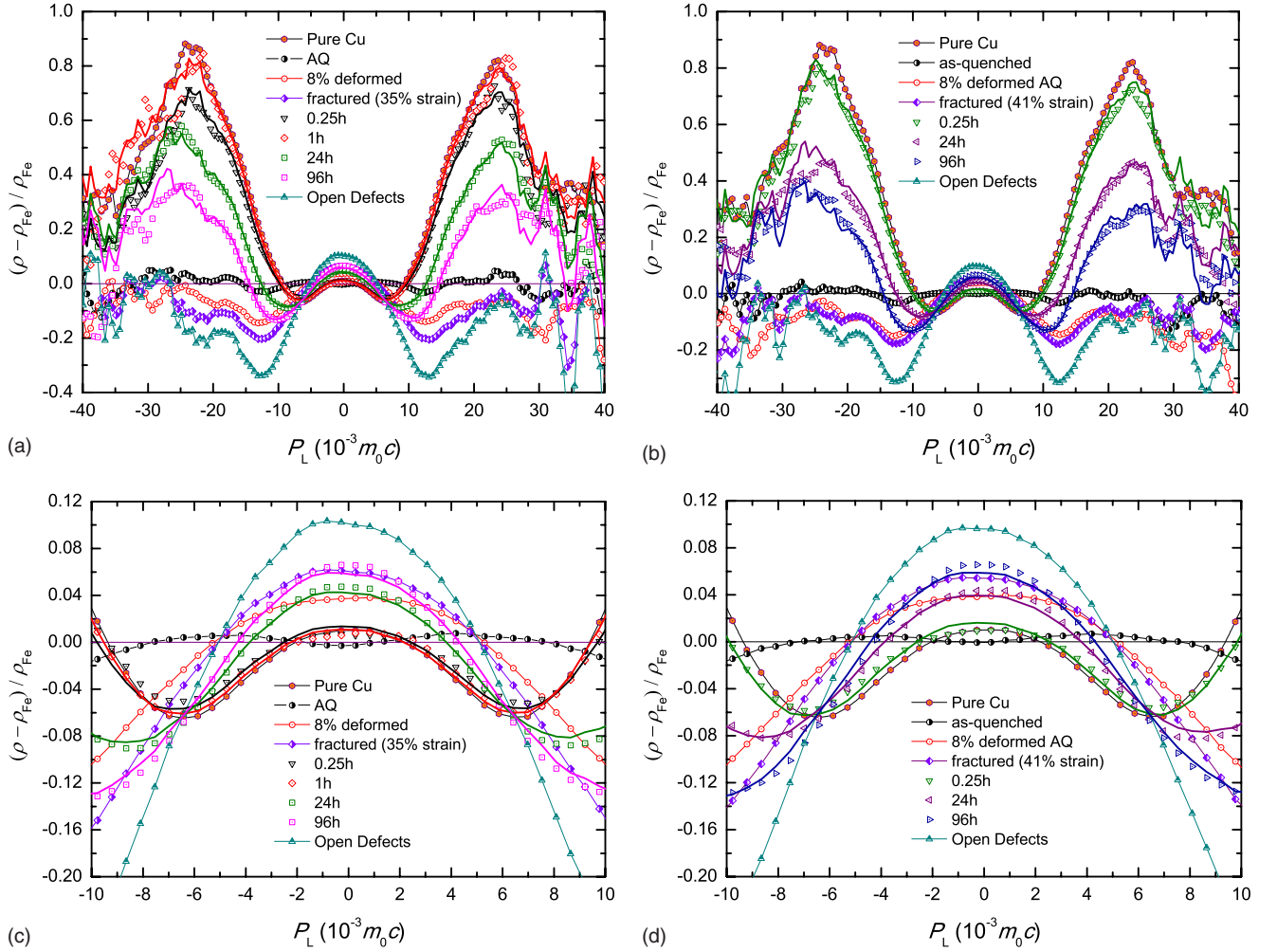


FIG. 6. (Color online) Evolution of the coincidence Doppler broadening relative to annealed iron  $(\rho - \rho_{\text{Fe}}) / \rho_{\text{Fe}}$  as a function of the electron momentum  $p_L$  for (a) the as-quenched Fe-Cu alloy and (b) the as-quenched Fe-Cu-B-N alloy during aging. The reference spectrum for pure copper is also shown. For clarity, enlargements of the low-momentum regions are shown for (c) the Fe-Cu alloy and (d) the Fe-Cu-B-N alloy.

aging response on the hardness shown in Fig. 2. For both alloys, the contribution from Cu decreases with the aging time (after reaching a peak), while the contribution from Fe increases with the aging time. Assuming that the chance that the positrons annihilate with either Fe or Cu atoms is about equal at the interface, this indicates that for longer aging times, the majority of the positron is trapped at the interface rather than inside the precipitates.

A quantitative chemical analysis of vacancy-solute complexes in aluminum alloys was first proposed by Somoza and co-workers<sup>37</sup> and further developed in later studies.<sup>38–40</sup> It was found that the CDB spectra for these alloys can be fitted accurately by a linear combination of the CDB spectra of annealed Al and those of the cold-worked pure metals present in the alloy.

The vacancy-formation behavior of iron alloys was however found to differ significantly from that of aluminum alloys. Unlike the obvious increase of the fraction of vacancies in (annealed) aluminum and aluminum alloys after quenching,<sup>41</sup> there is no distinct evidence for vacancy formation by quenching in iron and Fe-Cu alloys. Experimentally

it was found that the mean positron lifetime in pure iron remains unchanged when the quench temperature is varied from 650 to 1150 °C.<sup>33</sup> This is supported by our observation that the *S-W* couples of as-quenched and annealed pure iron are virtually identical and that the *S-W* couples of the as-quenched alloys are very close to that of annealed pure iron. This indicates that in iron alloys, it is very difficult to form open-volume defects or vacancy-solute complexes by thermal processing in the studied temperature range.

Here we use a similar fitting method to that has been presented by Somoza and co-workers.<sup>37</sup> The basis of the analysis is the assumption that the CDB spectrum of the alloy  $\rho_{\text{alloy}}$  can be fitted by a linear combination of reference spectra for the alloy components

$$\rho_{\text{Alloy}} = (1 - F)\rho_{\text{Matrix}}^{\text{Free}} + F(C_{\text{Cu}}\rho_{\text{Cu}}^{\text{Trap}} + C_{\text{Defects}}\rho_{\text{Defects}}^{\text{Trap}}), \quad (1)$$

where  $\rho_{\text{Matrix}}^{\text{Free}}$  is the reference spectrum for free positrons annihilating in the alloy matrix,  $\rho_{\text{Cu}}^{\text{Trap}}$  is the reference spectrum for annealed pure Cu, and  $\rho_{\text{Defects}}^{\text{Trap}}$  is the reference spectrum for open-volume defects in the alloy.  $F$  is a fraction of the

annihilated positrons trapped at Cu precipitates and/or open-volume defects (dislocations, vacancies, vacancy-solute complexes, and misfit regions at the matrix-precipitate interface). The remaining fraction  $(1-F)$  corresponds to positrons annihilating in the matrix of the alloy. From those positrons that are trapped, a fraction  $C_{\text{Cu}}$  annihilates with Cu electrons at the precipitates. A fraction  $C_{\text{Defects}}=1-C_{\text{Cu}}$  accounts for positrons annihilating with the open-volume defects. If one neglects the distortion of the positron wave function due to the different positron affinities with the different atoms in contact with the trap,  $C_{\text{Cu}}$  is equivalent to the fractional annihilation concentration of the Cu precipitates.

The experimental spectra for annealed pure iron ( $\rho_{\text{Fe}}^{\text{Free}} = \rho_{\text{Fe}}$ ) and annealed pure copper ( $\rho_{\text{Cu}}^{\text{Free}}$ ) were taken as references for  $\rho_{\text{Matrix}}^{\text{Free}}$  and  $\rho_{\text{Cu}}^{\text{Trap}}$ , respectively. Since the tensile deformation does not induce Cu precipitation in the as-quenched alloys ( $C_{\text{Cu}}=0$ ), the reference spectrum for open-volume defects in the alloy  $\rho_{\text{Defects}}^{\text{Trap}}$  is directly related to the experimental spectrum  $\rho_{\text{Fracture}}$  of the alloy sample that was deformed up to fracture. In terms of the relative difference with respect to the annealed iron spectrum  $\rho_{\text{Fe}}$ , we find

$$\left( \frac{\rho_{\text{Fracture}} - \rho_{\text{Fe}}}{\rho_{\text{Fe}}} \right) = F_{\text{Fracture}} \left( \frac{\rho_{\text{Defects}}^{\text{Trap}} - \rho_{\text{Fe}}}{\rho_{\text{Fe}}} \right), \quad (2)$$

where  $F_{\text{fracture}}$  is the fraction of positrons trapped at open-volume defects (vacancies, dislocations, and nanovoids) in the fractured sample. As not all positrons may be trapped in the fractured sample ( $F_{\text{fracture}} < 1$ ), we have estimated  $F_{\text{fracture}}$  from the experimental as-quenched alloy spectra at the maximum applied aging time of 96 h. At maximum aging, most of the supersaturated copper have precipitated and therefore all positions are expected to be trapped at Cu precipitates and/or open-volume defects in the alloy ( $F=1$ ). In terms of the relative difference with respect to the annealed iron spectrum  $\rho_{\text{Fe}}$ , this gives

$$\begin{aligned} \left( \frac{\rho_{\text{max aged}} - \rho_{\text{Fe}}}{\rho_{\text{Fe}}} \right) &= C_{\text{Cu,max aged}} \left( \frac{\rho_{\text{Cu}}^{\text{Trap}} - \rho_{\text{Fe}}}{\rho_{\text{Fe}}} \right) \\ &+ (1 - C_{\text{Cu,max aged}}) \left( \frac{\rho_{\text{Defects}}^{\text{Trap}} - \rho_{\text{Fe}}}{\rho_{\text{Fe}}} \right). \end{aligned} \quad (3)$$

Combining the experimental conditions at fracture [Eq. (2)] and at maximum aging [Eq. (3)], the parameter  $F_{\text{Fracture}}$  can be estimated for the studied samples:  $F_{\text{Fracture}}=0.60(2)$  for Fe-Cu, 0.56(1) for Fe-Cu-B-N, and 0.22(1) for pure Fe. With these parameters, the reference spectrum for open-volume defects  $\rho_{\text{Defects}}^{\text{Trap}}$  can be obtained for all samples. This reference spectrum  $\rho_{\text{Defects}}^{\text{Trap}}$  was subsequently used to calculate the reference points for open-volume defects, indicated in the  $S$ - $W$  plots of Fig. 5.

As illustrated in Fig. 7, the fraction  $F$  and the fractional contributions  $C_{\text{Cu}}=1-C_{\text{Defects}}$  were used as the fit parameters for a linear least-squares fit of the experimental spectrum to the reference spectra [Eq. (1)], neglecting the small contribution to annihilation spectrum originating from the minority alloying elements, such as B, N, and Ce. The calculated spectrum obtained from a linear fit of the reference spectra

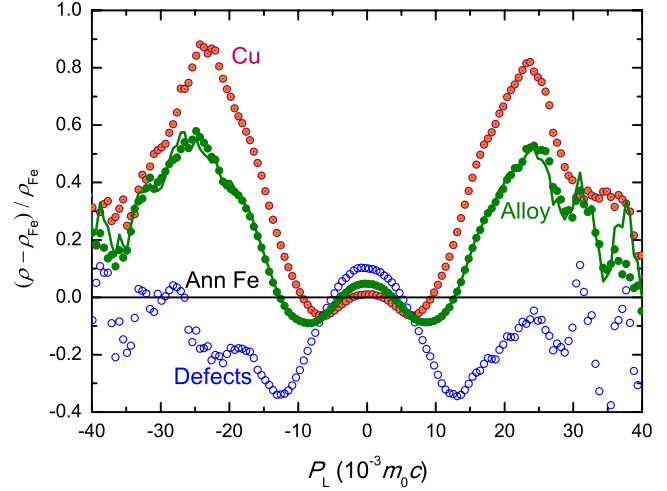


FIG. 7. (Color online) Coincidence Doppler broadening relative to annealed iron  $(\rho - \rho_{\text{Fe}}) / \rho_{\text{Fe}}$  as a function of the electron momentum  $p_L$  for the as-quenched Fe-Cu alloy aged for 24 h at 550 °C. Solid line indicates a fit of the data by a linear combination of the reference spectra obtained for pure Cu, annealed Fe, and defects in the Fe-Cu alloy.

closely resembles the measured data of the alloy in Fig. 7. The proposed linear decomposition of the annihilation spectra in reference spectra works remarkably well in both the high-momentum and the low-momentum regions for the Fe-Cu and Fe-Cu-B-N alloys.

Applying the above fitting method to the CBD spectra of Fig. 6, quantitative estimates for the fractional contributions are obtained. Figure 8 shows the fractional contribution of positrons annihilating at Cu precipitates ( $FC_{\text{Cu}}$ ), at open-volume defects ( $FC_{\text{Defects}}$ ), and in the matrix ( $1-F$ ) as a function of the aging time for the as-quenched and annealed alloys. In case of the as-quenched Fe-Cu alloy, the contribution of open-volume defects strongly increases by the tensile deformation to a value of 38% and nearly vanishes again (to a value of 5%) during the subsequent initial aging of 0.25–0.5 h. Simultaneously, the contribution of copper climbs quickly from zero to over 80% during aging, which implies that the open defects are mainly filled with copper precipitates. The decoration of dislocations by Cu precipitates during aging has been confirmed in complementary TEM observations on the same alloy. For longer aging times, the fractional contribution of copper reaches a maximum at 1 h and then decreases, while simultaneously the contribution of open defects exhibits a gradual increase. For the Fe-Cu-B-N alloy, the aging evolution of the fractional contributions to the CBD spectra show a similar behavior as that observed for Fe-Cu. The main difference lies in the time scales for the precipitation kinetics. For the as-quenched Fe-Cu-B-N alloy, the maximum contribution of copper and the minimum contribution of open-volume defects are both reached at the shortest annealing time of 0.25 h (and may even be reached before this time), which is significantly faster than in Fe-Cu. This difference in aging response is consistent with the results obtained in the hardness measurements on both alloys.

The annealed Fe-Cu and Fe-Cu-B-N alloys both show a lower fractional contribution from copper precipitates and

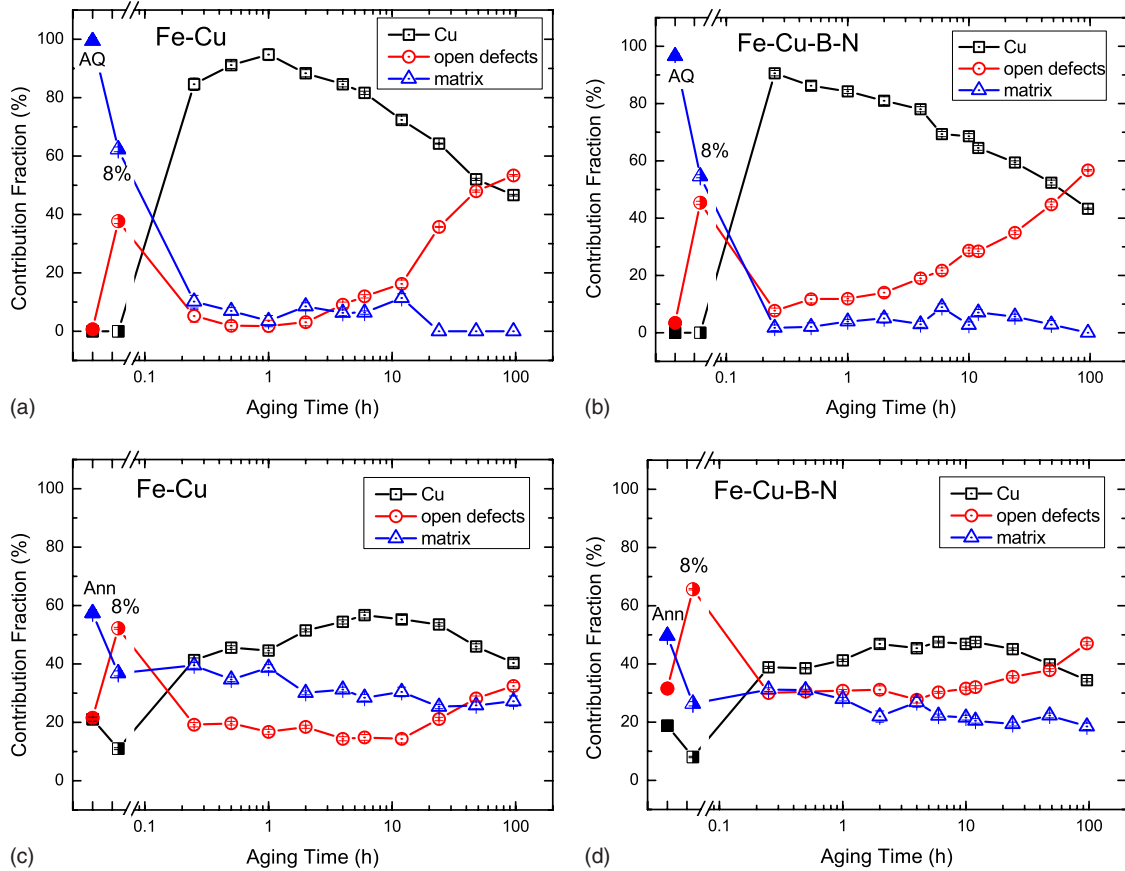


FIG. 8. (Color online) Evolution of the fractional contribution of Cu, open-volume defects, and free matrix positrons annihilation sites of the Fe-Cu and Fe-Cu-B-N alloys during aging for AQ and Ann samples.

open-volume defects. With deformation, new open-volume defects are created and subsequently removed again in the first aging step. The fractional contributions remain about constant during aging up to an aging time of 10 h. For longer aging times, the fractional contribution of open-volume defects increases, while the fractional contribution of Cu precipitates decreases for both the alloys. This indicates that although few new precipitates are expected to be formed in the annealed samples, a similar precipitate coarsening behavior for the present Cu precipitates is observed during the later aging stages, as found for the as-quenched samples. The annealed samples always show a considerable contribution from open-volume defects, which probably originates from a limited coherency of the relatively large Cu precipitates with the matrix. It is expected that the difference in solute concentration and mobility of Cu atoms in the as-quenched and annealed samples accounts for the difference in aging evolution of the open-volume defects. The as-quenched samples are initially in a supersaturated state with uniformly distributed Cu atoms showing a high mobility. In the annealed samples, however, most of the Cu solute are depleted due to the formation of relatively large fcc Cu precipitates that are incoherent with the matrix. The formed precipitates strongly reduce the mobility of the Cu atoms and have already introduced a misfit in the precipitate-matrix interface. In complementary optical microscopy studies on our Fe-Cu alloy, we found chains of coarse precipitates with a size larger than

2  $\mu\text{m}$  decorated along the grain boundaries in annealed samples, which were not present in the as-quenched samples. The results in Fig. 8 further indicate that the fractional contribution of the matrix is always higher in the annealed samples than in the as-quenched samples after aging. The presence of a low density of relatively large precipitates in the annealed samples may be responsible for this phenomenon. It is easy to understand that for larger precipitates, the mean distance between the precipitates is longer, resulting in a higher possibility that the positrons will annihilate with the electrons in the defect-free matrix.

#### IV. CONCLUSIONS

The isothermal precipitation in deformed Fe-Cu and Fe-Cu-B-N alloys is investigated with CDB spectroscopy and hardness test. The evolution of three contributions to positron annihilation spectra, i.e., open-volume defects, Cu precipitates, and Fe matrix, is characterized by extracting the *S-W* couples and by fitting the CDB spectra by a linear combination of reference spectra. CDB spectra were recorded before deformation, after deformation, and at different time intervals during the subsequent aging at 550 °C. The main conclusions are:

- (1) The addition of B and N to the Fe-Cu alloy significantly accelerates the Cu precipitation in the as-quenched

alloys, manifested by both the hardness tests and the positron annihilation spectroscopy.

(2) The shift in  $S$ - $W$  couples of the deformed samples with different strain levels shows a unique linear behavior for all samples:  $S$  increases and  $W$  decreases for increasing strain levels.

(3) During the initial stage of aging at 550 °C, the deformed as-quenched Fe-Cu and Fe-Cu-B-N alloys exhibit a sharp reduction in open-volume defects accompanied with a strong copper signature. This behavior is attributed to the closure of most of the open-volume defects introduced by plastic deformation by copper precipitation. We hereby demonstrated self-healing of damage in Fe-Cu and Fe-Cu-B-N systems.

(4) With further aging, the shift of the  $S$ - $W$  couples shows that new open-volume defects are generated for the Fe-Cu (after 1–2 h) and the Fe-Cu-B-N (after 0.25–0.5 h) alloys.

For both alloys, the formation of new open-volume defects is observed significantly before the peak hardness is reached during aging, indicating that beyond a critical size, the interface between the copper precipitates and the matrix gradually loses its coherency.

(5) After deformation, the annealed samples show a much slower evolution in the Cu precipitates during aging at 550 °C compared to the corresponding as-quenched samples. The open-volume defects in the annealed samples can only be reduced partially.

#### ACKNOWLEDGMENTS

This research was financially supported by the Innovation-Oriented Research Program on self-healing materials (IOP Project No. SHM0636) of the Dutch Ministry of Economic Affairs.

\*Corresponding author. FAX: +31(0)152788303; hsm3152k@yahoo.com.cn

- <sup>1</sup>K. Laha, J. Kyono, S. Kishimoto, and N. Shinya, *Scr. Mater.* **52**, 675 (2005).
- <sup>2</sup>N. Shinya, J. Kyono, and K. Laha, *J. Intell. Mater. Syst. Struct.* **17**, 1127 (2006).
- <sup>3</sup>K. Laha, J. Kyono, and N. Shinya, *Scr. Mater.* **56**, 915 (2007).
- <sup>4</sup>U. Dahmen, P. Ferguson, and K. H. Westmacott, *Acta Metall.* **32**, 803 (1984).
- <sup>5</sup>P. J. Othen, M. L. Jenkins, G. D. W. Smith, and W. J. Phythian, *Philos. Mag. Lett.* **64**, 383 (1991).
- <sup>6</sup>P. J. Othen, M. L. Jenkins, and G. D. W. Smith, *Philos. Mag. A* **70**, 1 (1994).
- <sup>7</sup>R. Monzen, M. L. Jenkins, and A. P. Sutton, *Philos. Mag. A* **80**, 711 (2000).
- <sup>8</sup>M. K. Miller, P. Pareige, and M. G. Burke, *Mater. Charact.* **44**, 235 (2000).
- <sup>9</sup>P. J. Pareige, K. F. Russell, and M. K. Miller, *Appl. Surf. Sci.* **94-95**, 362 (1996).
- <sup>10</sup>P. Pareige and M. K. Miller, *Appl. Surf. Sci.* **94-95**, 370 (1996).
- <sup>11</sup>D. Isheim, M. S. Gagliano, M. E. Fine, and D. N. Seidman, *Acta Mater.* **54**, 841 (2006).
- <sup>12</sup>G. M. Worrall, J. T. Buswell, C. A. English, M. G. Hetherington, and G. D. W. Smith, *J. Nucl. Mater.* **148**, 107 (1987).
- <sup>13</sup>K. Osamura, H. Okuda, M. Takashima, K. Asano, and M. Furusaka, *Mater. Trans., JIM* **34**, 305 (1993).
- <sup>14</sup>K. Osamura, H. Okuda, K. Asano, M. Furusaka, K. Kishida, F. Kurosawa, and R. Uemori, *ISIJ Int.* **34**, 346 (1994).
- <sup>15</sup>Y. Nagai, T. Chiba, Z. Tang, T. Akahane, T. Kanai, M. Hasegawa, M. Takenaka, and E. Kuramoto, *Phys. Rev. Lett.* **87**, 176402 (2001).
- <sup>16</sup>K. Sumiyama, Y. Yoshitake, and Y. Nakamura, *Acta Metall.* **33**, 1785 (1985).
- <sup>17</sup>P. Asoka-Kumar, B. D. Wirth, P. A. Sterne, R. H. Howell, and G. R. Odette, *Philos. Mag. Lett.* **82**, 609 (2002).
- <sup>18</sup>J. J. Blackstock and G. J. Ackland, *Philos. Mag. A* **81**, 2127 (2001).
- <sup>19</sup>Y. Le Bouar, *Acta Mater.* **49**, 2661 (2001).
- <sup>20</sup>J.-H. Shim, Y. W. Cho, S. C. Kwon, W. W. Kim, and B. D. Wirth, *Appl. Phys. Lett.* **90**, 021906 (2007).
- <sup>21</sup>E. Kozeschnik, *Scr. Mater.* **59**, 1018 (2008).
- <sup>22</sup>M. Legros, G. Dehm, E. Arzt, and T. J. Balk, *Science* **319**, 1646 (2008).
- <sup>23</sup>Y. Nagai, M. Hasegawa, Z. Tang, A. Hempel, K. Yubuta, T. Shimamura, Y. Kawazoe, A. Kawai, and F. Kano, *Phys. Rev. B* **61**, 6574 (2000).
- <sup>24</sup>T. Onitsuka, M. Takenaka, E. Kuramoto, Y. Nagai, and M. Hasegawa, *Phys. Rev. B* **65**, 012204 (2001).
- <sup>25</sup>Y. Nagai, Z. Tang, H. Ohkubo, K. Takadate, and M. Hasegawa, *Radiat. Phys. Chem.* **68**, 381 (2003).
- <sup>26</sup>M. Hasegawa, Z. Tang, Y. Nagai, T. Chiba, E. Kuramoto, and M. Takenaka, *Philos. Mag.* **85**, 467 (2005).
- <sup>27</sup>P. Hautojärvi and A. Vehanen, *Appl. Phys. (Berlin)* **11**, 191 (1976).
- <sup>28</sup>K. Petersen, I. A. Repin, and G. Trumphy, *J. Phys.: Condens. Matter* **8**, 2815 (1996).
- <sup>29</sup>S. Hautakangas, H. Schut, N. H. van Dijk, P. E. J. Rivera Diaz del Castillo, and S. van der Zwaag, *Scr. Mater.* **58**, 719 (2008).
- <sup>30</sup>A. Deschamps, M. Militzer, and W. J. Poole, *ISIJ Int.* **41**, 196 (2001).
- <sup>31</sup>A. Deschamps, M. Militzer, and W. J. Poole, *ISIJ Int.* **43**, 1826 (2003).
- <sup>32</sup>Y. Kamada, S. Takahashi, H. Kikuchi, S. Kobayashi, K. Ara, J. Echigoya, Y. Tozawa, and K. Watanabe, *J. Mater. Sci.* **44**, 949 (2009).
- <sup>33</sup>J. Topolsky, S. Y. Chuang, and S. J. Tao, *Phys. Status Solidi A* **35**, K17 (1976).
- <sup>34</sup>M. J. Puska, P. Lanki, and R. M. Nieminen, *J. Phys.: Condens. Matter* **1**, 6081 (1989).
- <sup>35</sup>N. F. Mott and F. R. N. Nabarro, *Report on Strength of Solids* (Phys. Soc., London, 1948).
- <sup>36</sup>Z. Tang, M. Hasegawa, Y. Nagai, and M. Saito, *Phys. Rev. B* **65**, 195108 (2002).
- <sup>37</sup>A. Somoza, M. P. Petkov, K. G. Lynn, and A. Dupasquier, *Phys. Rev. B* **65**, 094107 (2002).
- <sup>38</sup>P. Folegati, A. Dupasquier, R. Ferragut, M. M. Iglesias, I.

- Makkonen, and M. J. Puska, *Phys. Status Solidi C* **4**, 3493 (2007).
- <sup>39</sup>A. Dupasquier, R. Ferragut, M. M. Iglesias, M. Massazza, G. Riontino, P. Mengucci, G. Barucca, C. E. Macchi, and A. Somoza, *Philos. Mag.* **87**, 3297 (2007).
- <sup>40</sup>R. Ferragut, A. Dupasquier, C. E. Macchi, A. Somoza, R. N. Lumleyd, and I. J. Polmear, *Scr. Mater.* **60**, 137 (2009).
- <sup>41</sup>A. Calloni, A. Dupasquier, R. Ferragut, P. Folegati, M. M. Iglesias, I. Makkonen, and M. J. Puska, *Phys. Rev. B* **72**, 054112 (2005).